Physics Letters A 379 (2015) 1384–1390

Contents lists available at ScienceDirect

Physics Letters A

www.elsevier.com/locate/pla

Electronic structures and optical properties induced by silicon twin boundaries: The first-principle calculation

X.X. Liu [a], L.Z. Liu [a], X.L. Wu [a,b,*], Paul K. Chu [c]

[a] Key Laboratory of Modern Acoustics, MOE, Institute of Acoustics and Collaborative Innovation Center of Advanced Microstructures, National Laboratory of Solid State Microstructures, Nanjing University, Nanjing 210093, PR China
[b] Department of Physics, NingBo University, NingBo 315301, PR China
[c] Department of Physics and Materials Science, City University of Hong Kong, Tat Chee Avenue, Kowloon, Hong Kong, China

ARTICLE INFO

Article history:
Received 17 December 2014
Received in revised form 9 February 2015
Accepted 26 February 2015
Available online 3 March 2015
Communicated by L. Ghivelder

Keywords:
Twin structure
Electronic states
Optical properties

ABSTRACT

The defect states and optical absorption enhancement induced by twin boundaries in silicon are investigated by first-principle calculation. The defect states in the forbidden bands are identified and based on the established electronic structures, the dielectric functions and absorption coefficients are derived. An important result of our calculations is that visible light absorption by the twinning configuration is enhanced significantly, indicating that twinning structures possibly play an important role in silicon-based photovoltaic devices.

© 2015 Elsevier B.V. All rights reserved.

1. Introduction

The electronic and structural properties of defects in semiconductors have attracted much scientific interest and there are three basic types of defects in crystals: point defects, linear defects and planar defects. Grain boundaries as planar defects are frequently present in semiconductors and affect the mechanical, electronic, and optical properties. During the past decades, theoretical [1–6] and experimental [7–10] efforts have been paid to properties of grain boundaries in silicon. Twin boundaries as special defects in the family of grain boundaries have also been involved experimentally and theoretically. In III–V semiconductors GaAs, GaP, InAs, and InP nanowires, twin boundaries were observed and even fabricated controllably by adjusting the experimental parameters [11–13]. Similar twins have also been observed from nanowires and nanocrystals of II–VI semiconductors such as ZnS [14], CdS [15], ZnSe [16]. In spite of extensive research on advanced materials, silicon continues to be the most important semiconductor in microelectronics and even photovoltaics. Stacking faults exist in homoepitaxial Si films [17] and twinned epitaxial Si layers are synthesized [18], and high-resolution electron microscopy has been conducted to examine twins in multi-crystalline silicon [19], Si nanowires [20,21], and Si nanocrystals [22]. Twinning superlattices have also been observed from Si epitaxial layers [23–25]. In addition to experimental investigation, theoretical calculation has been conducted. The nonorthogonal-binding method [26], empirical pseudopotential method [27], and first-principle calculation [28] have been adopted to calculate the defect states and stacking-fault energy in silicon. For instance, twin boundaries in Si were studied by the density functional theory and tight binding model [29,30]. The electronic properties of twinning boundaries, stacking faults, and twinning superlattice in group IV and III–V semiconductors were derived by an empirical pseudopotential layer method [31] and twin boundaries and stacking faults in cubic SiC, Si, and C were studied in the first-principle framework in conjunction with the density-functional theory and local-density approximation [32,33]. Most of the theoretical derivations so far are mainly concerned with the defect formation energy and electronic structure of the twin boundary in silicon but the optical properties of the twining configuration in silicon have not been studied systematically despite their importance to fundamental physics and applications. In fact, optical properties of silicon have attracted intense interest and been investigated in many scientific fields such as optoelectronics and photovoltaics. To manipulate the optical properties of silicon, researchers have explored various structures of silicon, including impurity-related defect centers [43], nanowires [35], porous silicon [36], photonic crystal [37], superlattice [38] and others [39]. In recent years, nonlinear optical effects in silicon further offer

* Corresponding author at: Key Laboratory of Modern Acoustics, MOE, Institute of Acoustics and Collaborative Innovation Center of Advanced Microstructures, National Laboratory of Solid State Microstructures, Nanjing University, Nanjing 210093, PR China.
E-mail address: hkxlwu@nju.edu.cn (X.L. Wu).

http://dx.doi.org/10.1016/j.physleta.2015.02.042
0375-9601/© 2015 Elsevier B.V. All rights reserved.

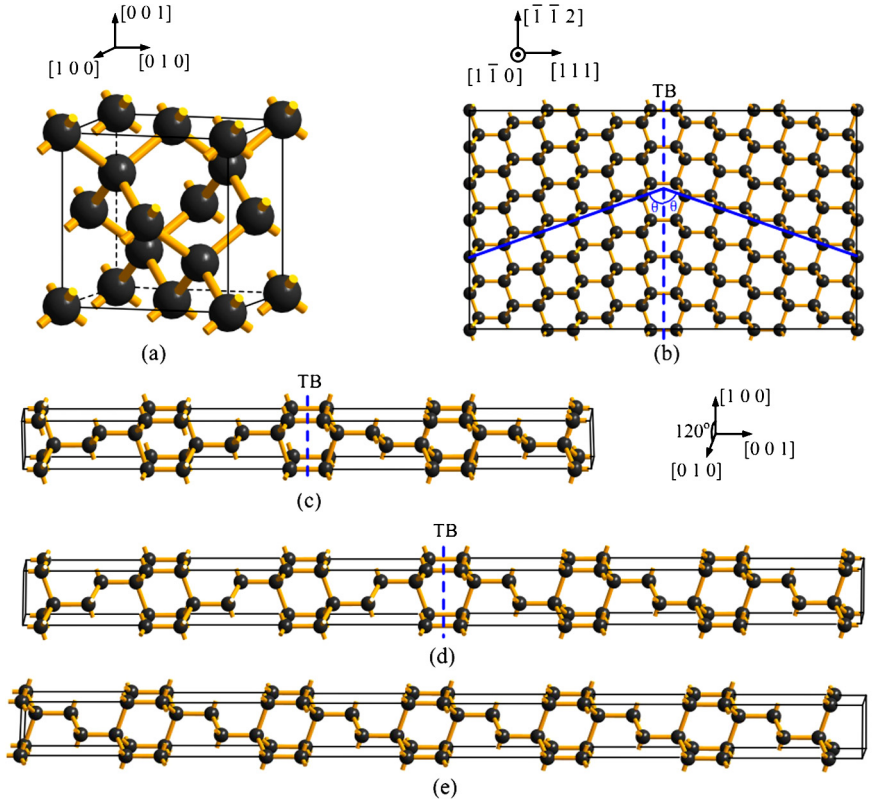

Fig. 1. (Color on-line.) (a) Atomic model of silicon with a diamond cubic crystal structure. (b) Twinned configuration with the twin boundary marked by the dotted line TB. (c) Twinned supercell containing 12 Si atomic bilayers and the twin boundaries are perpendicular to the [111] direction. (d) Twinned supercell containing 18 Si atomic bilayers. (e) Supercell of crystalline Si containing 18 Si atomic bilayers.

opportunities to generate the optoelectronic devices, the performance of which far exceeds those of the electronic devices [40]. In addition, silicon is the most important semiconductor materials in photovoltaics, so researchers have designed various structures to increase the absorption of sunlight in silicon. For example, Si nanowires offer new access to efficiently convert solar energy into electrical energy [41], and a new approach based on plasmonics has also been presented to reduce the thickness of absorber layers of solar cell [42].

The density functional method is quite prevalent in materials calculation and the increasing computing power has improved the accuracy. In the present work, we use the first-principle density functional method and plane-wave basis in combination with pseudo-potentials to calculate the electronic structures and optical properties of crystalline and twinning configurations in silicon. To determine the location of the interface states, we construct three geometric structures and calculate the energy bands and densities of states (DOSs). Owing to the good accuracy, the position of the defect states in the forbidden bands and changes of DOSs can be obtained. The optical properties of crystalline and twinned configurations in silicon such as the dielectric function and absorption coefficient are further derived. The optical absorption enhancement in the visible range due to the twin boundaries is demonstrated suggesting their potential role in improving light absorption in photovoltaic applications.

2. Calculations

We consider the silicon in the diamond structure [Fig. 1(a)] and the (111) plane and [111] direction are taken. Along the [111] direction, the normal stacking sequence is $\cdots AA'BB'CC'AA'BB'CC'\cdots$, where AA' (or BB', CC') represent the two basic atoms in the primitive unit cell [31]. However, the atomic stacking sequence changes in the presence of a twin boundary. The twinning configuration is comprised of the stacking sequence $\cdots AA'BB'CC'AA'CC'BB'AA'\cdots$. First of all, we cut the [111] directional bonds in the AA' layer and rotate half of the Si crystal by 180° to connect the two halves. We finally obtain the twin boundary, and do not change all the bond lengths and angles. One interface exists in the supercell of the twinned geometry as shown in Fig. 1(b). In the calculations, we utilize the package CASTEP (a supercell method) [44] in which all the studies are performed on a periodic system. We construct two supercells as shown in Fig. 1(c) and 1(d), in which the twin boundary is labeled TB. There are 6 and 9 atomic bilayers between two adjacent twin boundaries in Fig. 1(c) and 1(d), respectively. The model in Fig. 1(e) represents the crystalline silicon. The supercell in Fig. 1(c) consists of 48 silicon atoms and there are 72 silicon atoms in the supercell in Fig. 1(d) and 1(e).

We adopt the density functional approach based on the plane-wave basis set and pseudopotential to describe the electron–ion interaction (CASTEP code) [44]. The total energy of each geometry is calculated by generalized gradient approximation (GGA) in the framework of the Perdew–Burke–Eruzerhof (PBE) [45] exchange-correlation functional. The electron–ion interaction is described by the norm-conversing pseudopotential. The Si $3s^2p^2$ orbitals are treated as valence bands. To expand the plane-wave, the cut-off energies of crystalline and twinned silicon are set to 500 eV. Monkhorst and Pack [46] grid is used to sample the Brillouin zone, and the grid parameters are set to be $8\times8\times8$ for the primitive cell of silicon, $8\times8\times1$ for the twinned and crystalline supercells in Fig. 1(c), 1(d) and 1(e). We set the self-consistent field (SCF) tolerance 5.0×10^{-7} eV/atom in the energy calculation. To get the minimum-energy geometry, we optimize all the supercells and relax all the atoms. By utilizing the optimized geometries, the electronic structures and optical properties are calculated.

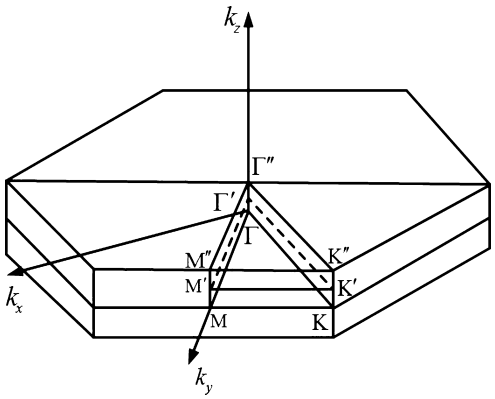

Fig. 2. First Brillouin zone (FBZ) of the supercell in Fig. 1(d). The high symmetry points Γ, M, K in reciprocal space are indicated. The axis k_z is parallel to the [111] direction of silicon.

3. Results and discussion

3.1. Electronic structures

In order to confirm the possible interface states in the fundamental gap due to the twin boundary, we compare the electronic structures of crystalline and twinning configurations of silicon. The first Brillouin zone (FBZ) of supercell is shown in Fig. 2. The energy bands are calculated along the high symmetrical directions Γ–M–K–Γ. In practice, the finite length of the supercell used in the calculation along the [111] direction, which is parallel to k_z, leads to slight variations in the energy bands along that direction. In fact, the longer the supercell along the [111] direction used in the calculation, the smaller is the FBZ along the k_z direction. We select two paths along Γ′–M′–K′–Γ′ and Γ″–M″–K″–Γ″ as shown in Fig. 2. The three points M′, K′, Γ′ are the midpoints of the segments MM″, KK″, ΓΓ″. We calculate the energy bands along the two paths and compare their difference with the band along Γ–M–K–Γ. It is found that the difference is little enough so that it can be ignored. In practice, we need only to calculate the energy dispersion relationship along Γ–M–K–Γ. In addition, we compare the differences of energy bands of the two supercells in Fig. 1(d) and 1(e), which contain same number of Si atoms.

The energy bands of crystalline silicon are calculated as shown in Fig. 3(a) and compared with the band structures reported by previous researchers. The band structures from our calculations are good consistent with those from previous theoretical [47–49] and experimental [48,50] results. The band gap calculated by the traditional DFT is underestimated substantially [51,52]. For insulators and semiconductors, the introduction of scissors is an effective approach to correct the DFT band gap [53,54]. The scissor corrects the band gap by shifting the conduction band with respect to the valence band. If we have the accurate experimental band gap of silicon, this approach produces good results. By comparing the band gap of silicon (1.12 eV) and our calculated result (0.64 eV), the scissor operator is set at 0.48 eV. Two kinds of twinning configurations are constructed and geometrically optimized to derive the band structures and DOSs. We use “Si twin66”, “Si twin99” and “Si bulk” to represent the three supercells in Fig. 1(c), 1(d) and 1(e). The calculated energy bands of “Si twin66” and “Si twin99” are shown in Fig. 3(c) and 3(d). Their band structures, especially in the valence band, are quite similar. The conduction band shows the same characteristics and furthermore, the band gaps of the two twinned structures are almost equal. It can be concluded that when two boundaries in the twinned configuration are separated by six atomic bilayers, the interaction is so little that they do not affect each other. The conclusion is consistent with previous results [31,33]. Therefor, we compare the band structures of “Si twin99” and “Si bulk” shown in Fig. 3(b). Up to now, researchers have developed several other functionals to overcome the limitations of DFT such as screen-exchange LDA (sX-LDA) [55] and hybrid (HSE06) [56] functionals. The GW [57] method can yield very accurate band structures, but it is very time-consuming. In order to test the validity of the result from GGA, we adopt sX-LDA to re-calculate the energy bands for crystalline silicon (see Supplementary Information, Fig. S1). The bandgap of silicon from sX-LDA is 1.05 eV which is very close to the experimental value 1.12 eV. By the same way, we adopt sX-LDA to re-calculate the energy bands of “Si twin66” and “Si bulk” (see Supplementary Information, Fig. S2). It is found that the interface states near Γ are still located at

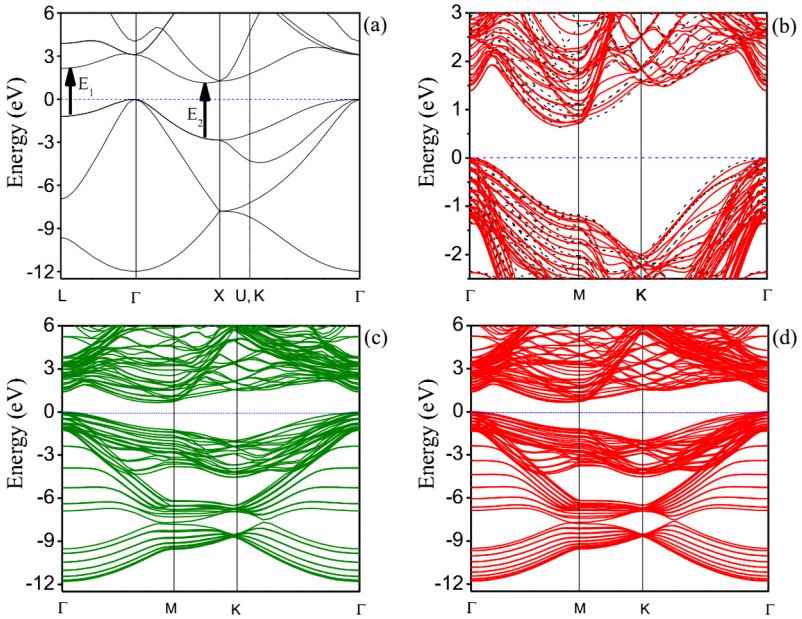

Fig. 3. (Color on-line.) (a) Band structures of silicon derived from our calculation. The k-point path is along L–Γ–X–U K–Γ. The arrows E_1 and E_2 represent the intervals of the bands. (b) Band structures of the Si supercell in Fig. 1(e) (black dash lines) and twinned supercell in Fig. 1(d) (red lines) with energies from −2.5 to 3.0 eV. They are plotted for identifying the interface states. (c) Band structures of the twinned supercell in Fig. 1(c) (olive lines) with energies from −12.5 to 6.0 eV. (d) Band structures of the twinned supercell in Fig. 1(d) (red lines) with energies from −12.5 to 6.0 eV.

0.10 eV below the bottom of conduction bands. Most importantly, the structures near the forbidden bands from GGA and sX-LDA are similar. Thus, the scissor operator is indeed an effective approach to correct the band gap for silicon, and meanwhile gives correct results. In addition, compared to sX-LDA, GGA is able to save time significantly. Since the band structures obtained with our calculation method are reliable, our calculations in optical properties of twinning configurations should also be correct. In the following, we analyze all the calculation results from GGA.

Compared to a perfect crystal, the twinning configuration does not keep the translational invariance along the [111] direction. Of course, the wave functions at the interface comply the symmetry parallel to the interface but the translational invariance perpendicular to the interface is broken. This symmetry breaking can actually lead to new solutions of the Kohn–Sham equation for electronic states only at the interface. The bond length and bond angle of silicon are 2.371 Å and 109.471°. The difference of the bond angle between the crystalline and twinned silicon is less than 0.1°. The mutually exclusive potentials on both sides of the interface are generated to stretch the bonds across the interface. The bonds across the twin interface in "Si twin99" are obviously elongated from 2.371 to 2.387 Å, whereas the other bonds vary slightly. The changes of the bonds in "Si twin66" have similar characteristics. We give the exact bond lengths and angles in "Si twin66" in the Supplementary Information, Fig. S3. These changes of bond length and angle can be categorized as the structural relaxation effect.

To determine the existence of interface bound states in the twinning configurations, we compare the differences of energy bands of "Si twin99" and "Si bulk" along Γ–M–K–Γ in Fig. 3(b). The red lines represent the energy bands of "Si twin99", while the black dash lines belong to "Si bulk". In order to identify the exact location of interface states, we only plot the energy bands from −2.5 to 3.0 eV. On the edges of conduction-band and valence-band, the red curves below and above the black dash curves denote the defect states related to the twin boundary, respectively. Near the energy gap, defect states are found near Γ, M, and K below the conduction band edge and near K above the valence band edge. The interface states are mainly located at Γ and 0.10 eV below the bottom of conduction bands.

There are different views on the position of the interface states. Early calculation by the nonorthogonal-tight-binding (NTB) [26] and empirical pseudopotential [27] methods reveals that the position of the interface states near Γ is 0.10 eV above the valence band edge, while subsequent first-principle [28] and other calculation [58] shows that the interface states reside at 0.10 eV below the bottom of the conduction bands. Experimental result [59] furnishes evidence of the state 0.10 eV below the conduction band edge which is indicated by our calculation. The early calculation methods such as NTB and empirical pseudopotential have some deficiencies. NTB is suitable for valence band structure calculation but cannot yield the accurate conduction band structure. Similarly, the empirical pseudopotential method cannot provide the interface states at the bottom of the conduction band because of limited fitting parameters. It is difficult to identify the presence of defect states because they are very close to the states on the conduction-band and valence-band edges of crystalline silicon. However, we are able to identify the presence of defect states because of the better accuracy in the DFT scheme.

The DOSs are shown in Fig. 4. The calculated DOS for crystalline silicon is consistent with the experimental [60] and theoretical [47] DOS. Based on the same accuracy, the DOSs of "Si twin66" and "Si twin99" are calculated and the three kinds of DOSs are compared. As shown in Fig. 4(a), the two curves of the twinning configurations are very similar but different from that of crystalline silicon. In order to determine the influence of the twin boundary on the DOS, the DOSs of the crystalline and twinning configurations from

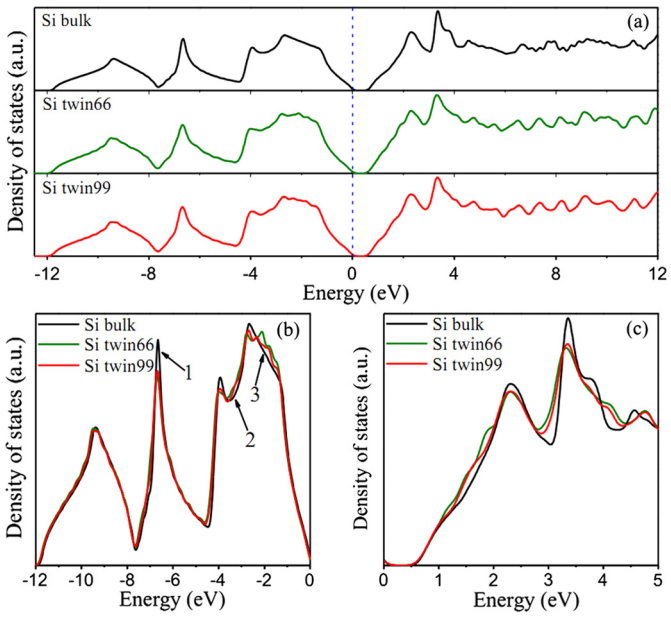

Fig. 4. (Color on-line.) (a) DOSs of the crystalline and twinning configurations of silicon in the energy range from −12.0 to 12.0 eV. (b) Comparison of the DOSs of the crystalline and twinned silicon in the energy range between −12.0 and 0 eV. The difference is indicated by arrows 1, 2, and 3. (c) Comparison of the DOSs in the energy range between 0 and 5.0 eV.

−12.0 to 0 eV and from 0 to 5.0 eV are shown in Fig. 4(b) and 4(c), respectively. The regions around the valleys of the valence band density of states are affected when the bond length and angle deviate from the ideal crystalline state [47]. It is somewhat different from the situation when a twin boundary exists. The atomic arrangement along the [111] is changed but no dangling bonds are introduced and the bond length or angle remains unchanged. The twin interface does not introduce states at the bottom of the left valley, however the right valley is somewhat filled. The height of the peak around −7.4 eV is reduced labeled by the arrow 1 in Fig. 4(b). Furthermore, the presence of the twin boundary also influences these two peaks of crystalline silicon appearing around −4.0 and −2.0 eV, as indicated by the arrows 2 and 3 in Fig. 4(b). The surface could introduce a peak in the middle of forbidden bands where DOS is equal to naught in the ideal crystal. However, the twin interface does not because the twin boundary does not deviate from the ideal crystal substantially. The DOSs of the crystalline and twinned configurations of silicon at the bottom of conduction bands are compared in Fig. 4(c) and there is no significant difference. Therefore, the twin interface does not influence the DOS much, implying that the interface states account for a small portion of the total states at the bottom of conduction bands. Nevertheless, the optical properties may be affected significantly.

3.2. Optical properties

Considering that the optical properties of silicon are determined by the electronic structure, it is believed that the twin boundary has significant influence on the optical properties, because the electronic structure of the twinning configuration is different from that of crystalline silicon. Hence, the optical constants, including the dielectric function and absorption coefficient, are calculated. The imaginary part $\varepsilon_2(\omega)$ of the dielectric function $\varepsilon(\omega)$ can be derived from the momentum matrix elements between the wave functions belonging to conduction and valence bands restricted by the selection rules [34] and described by the following two equations [61,62]:

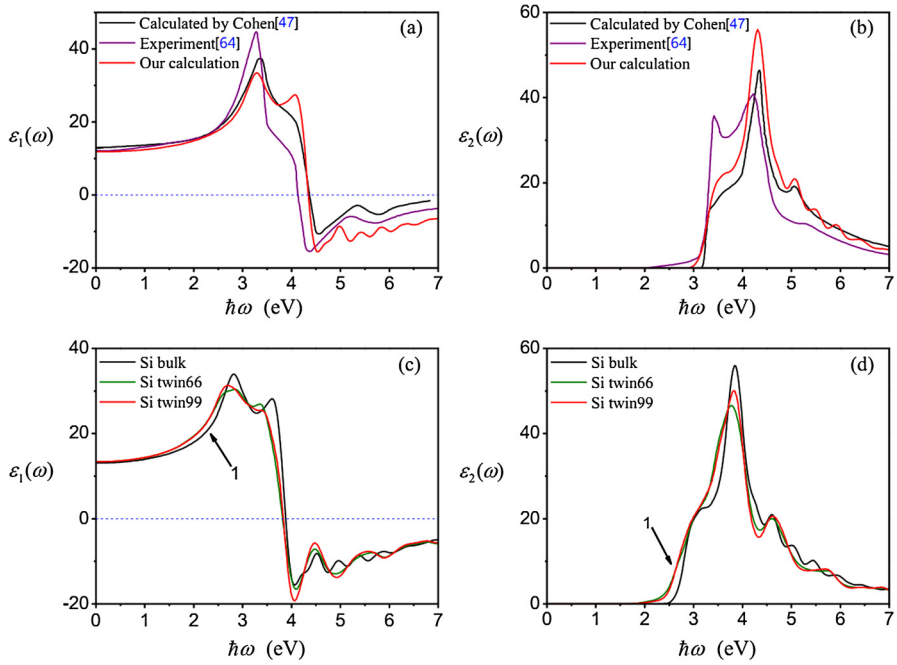

Fig. 5. (Color on-line.) (a) Real part of the dielectric function of silicon compared to experimental [64] and theoretical result [47]. (b) Imaginary part of the dielectric function of silicon compared to experimental [64] and theoretical result [47]. (c) Real part of the dielectric function of crystalline and twinned silicon from our calculation. (d) Imaginary part of the dielectric function of crystalline and twinned silicon from our calculation.

$$\varepsilon_2(\omega) = \frac{2e^2\pi}{\Omega\varepsilon_0}\sum_{\vec{k},c,v}\left|\left\langle\Psi_{\vec{k}}^{c}\middle|\vec{u}\cdot\vec{r}\middle|\Psi_{\vec{k}}^{v}\right\rangle\right|^2\delta\left(E_{\vec{k}}^{c}-E_{\vec{k}}^{v}-\hbar\omega\right) \tag{1}$$

$$\left\langle\Psi_{\vec{k}}^{c}\middle|\vec{u}\cdot\vec{r}\middle|\Psi_{\vec{k}}^{v}\right\rangle = \frac{1}{im\omega}\vec{u}\cdot\left\langle\Psi_{\vec{k}}^{c}\middle|\vec{P}\middle|\Psi_{\vec{k}}^{v}\right\rangle + \frac{1}{\hbar\omega}\vec{u}\cdot\left\langle\Psi_{\vec{k}}^{c}\middle|\left[|V_{nl}|,\vec{r}\right]\middle|\Psi_{\vec{k}}^{v}\right\rangle \tag{2}$$

where $\hbar\omega$ is the energy of the incident photon, e is the electron charge, Ω is the primitive cell volume, ε_0 is the vacuum permittivity, $\vec{u}$ is the polarization vector of the incident electric field, $\vec{r}$ is the position vector of electron, and $E_{\vec{k}}^{c}$ and $E_{\vec{k}}^{v}$ are the eigenvalues of wave functions $\Psi_{\vec{k}}^{c}$ and $\Psi_{\vec{k}}^{v}$ of the conduction and valence bands, respectively. $\vec{P}$ is the momentum operator and V_{nl} is the pseudopotential. The real part $\varepsilon_1(\omega)$ is obtained from the imaginary part $\varepsilon_2(\omega)$ of the dielectric function $\varepsilon(\omega)$ by the Kramer–Kronig relationship in Eqs. (3) and (4) where P represents the principle part of the integral. All the other optical constants such as the complex refractive index $\tilde{n}$, and absorption coefficient α can be derived from ε_1 and ε_2.

$$\varepsilon_1(\omega) - 1 = \frac{1}{\pi}P\int_{-\infty}^{\infty}\frac{\varepsilon_2(\omega')}{\omega'-\omega}d\omega', \tag{3}$$

and

$$\varepsilon_2(\omega) = -\frac{1}{\pi}P\int_{-\infty}^{\infty}\frac{\varepsilon_1(\omega')-1}{\omega'-\omega}d\omega'. \tag{4}$$

The optical properties are actually calculated for plane polarized light with the polarization direction [100], which is perpendicular to c-axis of the supercell. When we calculate the imaginary part of the dielectric function, the scissor operator is set at 0.48 eV because of the underestimation of the band gap by the GGA scheme. To corroborate the validity of the dielectric function, the dielectric function derived from our calculation is compared to previous theoretical [47,63] and experimental [64,65] results. The empirical pseudopotential method [47] and analytical-model approach [63] provide satisfactory results, however, the methods both involve the fitting parameters from experiments. The norm-conversing pseudopotential (NCPP) in our calculations comes from atomic potential and does not need any experimental parameters, which is a kind of *ab initio* pseudopotential. The accuracy of NCPP makes it widely used in the modern DFT softwares. As shown in Fig. 5(b), the configurations of the curves $\varepsilon_2(\omega)$ obtained by Cohen [47] and us are basically similar, although there is a fairly big discrepancy between the experimental and theoretical curves at around 3.5 eV. It has been suggested that the excitonic behavior rather than the local fields [66,67] is responsible for the difference [47]. It should be noted that the analogous discrepancy can also be observed from the curves $\varepsilon_1(\omega)$ in Fig. 5(a). Overall, the dielectric function from our calculation is sufficiently accurate to determine the other optical constants such as the absorption coefficient. To understand the extent to which the twinning configuration affects the optical properties of crystalline silicon, we are more concerned with $\varepsilon_2(\omega)$ because the imaginary part of the dielectric function directly represents the optical transitions between the valence and conduction bands. Fig. 5(d) displays the relationship between the imaginary part of the dielectric function and incident photon energy showing some distinctive features. The two curves corresponding to the twinned configurations almost overlap but they are different from the third curve. The twin interface does not change the position of the two main peaks of silicon at 3.68 eV (3.2 + 0.48 eV) and 4.31 eV (3.83 + 0.48 eV) but the intensity of highest peak is reduced. When the energy of the incident photon is less than 3.28 eV (2.80 + 0.48 eV), the intensity of $\varepsilon_2(\omega)$ of the twinning configuration is larger than that of $\varepsilon_2(\omega)$ of crystalline silicon. This is indicated by the arrow 1 in Fig. 5(d). Hence, the twin interface may be able to improve the probability of the optical transitions. The real part of the dielectric function $\varepsilon_1(\omega)$ is shown in Fig. 5(c). The two curves of the twinning configuration also coincide with each other and the intensity is larger than that of crystalline silicon indicated by the arrow 1 in Fig. 5(c).

In order to determine the energy range in which absorption is enhanced significantly, the curves of the absorption coefficient

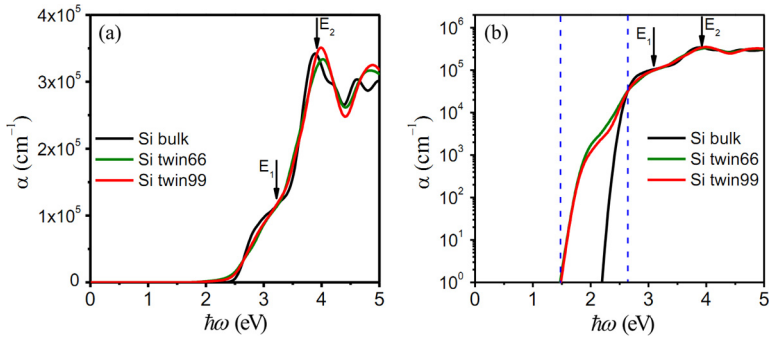

Fig. 6. (Color on-line.) (a) The calculated absorption coefficient of crystalline and twinned silicon. The two main peaks labeled with E_1 and E_2 correspond to the transitions between the conduction and valence bands in Fig. 3(a). (b) The calculated absorption coefficient of crystalline and twinned silicon in logarithmic coordinates.

versus incident photon energy are presented in Fig. 6(a). The two main peaks labeled E_1 and E_2 correspond to 3.20 and 4.00 eV, respectively and the distance between E_1 and E_2 remains 0.80 eV when comparing the curves from our computation and experiments [68]. Considering that the energy of peak E_1 is just 0.30 eV less than that of the peak in the experimental curve, the scissor operator is set at 0.30 eV. The scissor operator of α is different from that of $\varepsilon_2(\omega)$, because α is not proportional to $\varepsilon_2(\omega)$. As shown in Fig. 6(b), the logarithmic scale is adopted to show the relationship between the absorption coefficient and incident photon energy in order to indicate the change more clearly. If we assume that when α is less than 1 cm^{-1}, the absorption enhancement is not significant, the minimum energy 1.80 eV (1.50+0.30 eV) is determined by the blue dash line on the left. The blue dash line on the right indicates an energy of 2.94 eV (2.64+0.30 eV) for the incident photon when the absorption coefficients of crystalline and twinning configuration are equal. The curve of silicon and horizontal axis intersect at 2.50 eV (2.20 + 0.30 eV) as shown in Fig. 6(b). In the energy range between 1.80 and 2.50 eV, the absorption coefficient of the twinning configuration increases drastically when the energy of the incident phonon becomes larger. Meanwhile the absorption coefficient of crystalline silicon remains less than 1 cm^{-1}. In the energy range between 2.50 and 2.94 eV, the absorption coefficient of crystalline silicon is still less than that of the twinning configuration but increases rapidly to the point where they are equal. The energies at 1.80 and 2.94 eV correspond to the incident light wavelengths of 689 and 422 nm, respectively. The incident light between 422 and 689 nm is absorbed more strongly by the twin boundary in silicon. Considering that the visible spectrum of sunlight spans from 400 to 700 nm and the visible range also represents the strongest output of the total irradiance spectrum of the sun, the twin interface can enhance sunlight absorption and has potential applications in the field of photovoltaics. In fact, Lai et al. [69] showed that optical absorption was indeed enhanced by mechanical twins in low-temperature silicon epitaxial layer and it was attributed to the fact that the twins increase the optical path length consequently improving absorption. However, optical propagation modes are not limited to a special direction in a crystal. Thus, we believe that this geometrical interpretation is not appropriate for the increased absorption. Our calculation shows that absorption is strongly enhanced in the visible range. Although twins do alter optical absorption, it is our belief that the main reason why absorption is enhanced is not the longer light path but instead the presence of interface states and more intense interband transitions.

As a kind of extended defect, the twin boundary induces the shallow states near conduction band and valence band edges. In fact, the twin boundary defects are different from the common defects (e.g. impurities and vacancies). The latter introduce deep states in the gap because of severe lattice distortion or dangling bonds, which always degrade the PV performances. The twin boundaries do not introduce dangling bonds, and only change the crystal symmetry of silicon along special direction. Actually the twin boundary can enhance the optical absorption and does not degrade the photovoltaic performances, because the shallow energy levels does not become the effective carrier recombination centers. Since the practical applications in photovoltaics always involve dopants and intrinsic defects in silicon, it is necessary to investigate the interactions of the dopant atoms or vacancies with the twin boundaries.

Fazzio et al. have investigated the interaction of point defects with an intrinsic stacking fault in silicon [70] and the effects of stacking faults on the properties of dopants in GaAs [71]. Their studies focus on the changes of formation energy when the point defects are at different sites in the materials. With these results, they determined the favorable positions of defects in thermodynamic equilibrium conditions. However, we currently pay more attention to the influence of defects on optical properties of twinned silicon. An orthorombic supercell containing 68 atoms is used in our calculation. The dopants (boron and phosphorus atoms) and vacancy are in and further away from the twin boundaries, respectively (see Supplementary Information, Fig. S4). We calculate and compare the absorption coefficient of these structures (see Supplementary Information, Fig. S5). The substitutional boron and phosphorus atoms do not affect the absorption of the twinned silicon in the visible range, although the absorption enhances in the infrared spectral region near 0.70 eV (0.40 + 0.30 eV). The vacancies in different sites both enhance the absorption in the visible and infrared regions. In summary, the substitutional dopant and vacancy do not reduce the absorption induced by the twin boundaries in the visible range. Compared with the other methods for improving optical absorption in silicon solar cell (e.g. plasmonic structures and nanowires), twinning configuration does not involve the design of complicated structures. This advantage offers convenience and should make it an effective approach to enhance absorption in silicon-based photovoltaic devices.

4. Conclusion

We have utilized the first-principle density functional package CASTEP to calculate the energy bands, DOSs and optical properties of the crystalline and twinned silicon. After the geometry optimization, the bonds across the twinned boundary are stretched perpendicular to the interface. This implies that the mutually exclusive potentials on both sides of the interface are generated. Electronic defect states are identified by comparing the projected bulk bands of silicon and energy bands of the twinned silicon. The accurate positions of the interface states are designated. The influence on the DOS is mainly in the valence bands and the difference near the conduction band edge is not obvious. The optical absorption coefficient increases drastically in the visible range due to the

transitions between the conduction and valence bands. The vacancies and dopants commonly present in silicon do not reduce the enhanced absorption of visible light induced by the twin boundaries. The twinning structures possibly play an important role in silicon-based photovoltaic devices.

Acknowledgements

This work was jointly supported by Grants (Nos. 2011CB922102 and 2013CB932901) from the National Natural Science Foundation of China and Basic Research Programs of China and Jiangsu Province Natural Science Foundation (No. BK20130549). Partial support was also provided by the Guangdong–Hong Kong Technology Cooperation Funding Scheme (TCFS) No. GHP/015/12SZ. We also acknowledge computational resources of High Performance Computing Center of Nanjing University.

Appendix A. Supplementary material

Supplementary material related to this article can be found online at http://dx.doi.org/10.1016/j.physleta.2015.02.042.

References

[1] W.L. Huang, W. Ge, C.X. Li, C.F. Hou, X.W. Wang, X.F. He, Comput. Mater. Sci. 58 (2012) 38.
[2] J. Zhang, C.Z. Wang, K.M. Ho, Phys. Rev. B 80 (2009) 174102(1).
[3] S.V. Alfthan, K. Kaski, A.P. Sutton, Phys. Rev. B 74 (2006) 134101(1).
[4] K. Uchida, S. Tsuneyuki, Appl. Surf. Sci. 190 (2002) 129.
[5] F. Cleri, P. Keblinski, L. Colombo, S.R. Phillpot, D. Wolf, Phys. Rev. B 57 (1998) 6247.
[6] M. Kohyama, R. Yamamoto, Phys. Rev. B 50 (1994) 8502.
[7] Y. Ohno, K. Inoue, Y. Tokumoto, K. Kutsukake, I. Yonenaga, N. Ebisawa, H. Takamizawa, Y. Shimizu, K. Inoue, Y. Nagai, H. Yoshida, S. Takeda, Appl. Phys. Lett. 103 (2013) 102102(1).
[8] M. Rumler, M. Rommel, J. Erlekampf, M. Azizi, T. Geiger, A.J. Bauer, E. Meißner, L. Frey, J. Appl. Phys. 112 (2012) 034909(1).
[9] K. Kutsukake, N. Usami, K. Fujiwara, Y. Nose, K. Nakajima, J. Appl. Phys. 101 (2007) 063509(1).
[10] J. Chen, T. Sekiguchi, D. Yang, F. Yin, K. Kido, S. Tsurekawa, J. Appl. Phys. 96 (2004) 5490.
[11] F.M. Davidson, D.C. Lee, D.D. Fanfair, B.A. Korgel, J. Phys. Chem. C 111 (2007) 2929.
[12] P. Caroff, K.A. Dick, J. Johansson, M.E. Messing, K. Deppert, L. Samuelson, Nat. Nanotechnol. 4 (2009) 50.
[13] R.E. Algra, M.A. Verheijen, M.T. Borgström, L.F. Feiner, G. Immink, W.J.P. van Enckevort, E. Vlieg, P.A.M. Bakkers, Nature 456 (2008) 369.
[14] Y.F. Hao, G.W. Meng, Z.L. Wang, C.H. Ye, L.D. Zhang, Nano Lett. 6 (2006) 1650.
[15] P.Q. Zhao, S.J. Xiong, X.L. Wu, P.K. Chu, Appl. Phys. Lett. 100 (2012) 171911(1).
[16] Y.Q. Wang, U. Philipose, T. Xu, H.E. Ruda, K.L. Kavanagh, Semicond. Sci. Technol. 22 (2007) 175.
[17] R.N. Thomas, M.H. Francombe, Surf. Sci. 25 (1971) 357.
[18] H. Hibino, K. Sumitomo, T. Ogino, J. Vac. Sci. Technol., A, Vac. Surf. Films 16 (1998) 1934.
[19] K. Scheerschmidt, M. Werner, Phys. Status Solidi A 202 (2005) 2368.
[20] A.H. Carim, K.K. Lew, J.M. Redwing, Adv. Mater. 13 (2001) 1489.
[21] Q. Tang, X. Liu, T.I. Kamins, G.S. Solomon, J.S. Harris, Appl. Phys. Lett. 81 (2002) 2451.
[22] Y.Q. Wang, R. Smirani, G.G. Ross, Nano Lett. 4 (2004) 2041.
[23] H. Hibino, T. Ogino, Mater. Sci. Eng. B 87 (2001) 214.
[24] A. Fissel, E. Bugiel, C.R. Wang, H.J. Osten, Mater. Sci. Eng. B 134 (2006) 138.
[25] A. Fissel, E. Bugiel, C.R. Wang, H.J. Osten, J. Cryst. Growth 290 (2006) 392.
[26] L.F. Mattheiss, J.R. Patel, Phys. Rev. B 23 (1981) 5384.
[27] S. Marklund, Phys. Status Solidi B 108 (1981) 97.
[28] M.Y. Chou, M.L. Cohen, S.G. Louie, Phys. Rev. B 32 (1985) 7979.
[29] D.P. DiVincenzo, O.L. Alerhand, M. Schlüter, J.W. Wilkins, Phys. Rev. Lett. 56 (1986) 1925.
[30] M. Kohyama, R. Yamamoto, Y. Watanabe, Y. Ebata, M. Kinoshita, J. Phys. C 21 (1988) L695.
[31] Z. Ikonić, G.P. Srivastava, J.C. Inkson, Phys. Rev. B 48 (1993) 17181.
[32] P. Käckell, J. Furthmüller, F. Bechstedt, Phys. Rev. B 58 (1998) 1326.
[33] H.P. Iwata, U. Lindefelt, S. Öberg, P.R. Briddon, Phys. Rev. B 68 (2003) 113202(1).
[34] J. Palm, F. Gan, B. Zheng, J. Michel, L.C. Kimerling, Phys. Rev. B 15 (1996) 17603.
[35] P.R. Bandaru, P. Pichanusakorn, Semicond. Sci. Technol. 25 (2010) 024003.
[36] O. Bisi, S. Ossicini, L. Pavesi, Surf. Sci. Rep. 38 (2000) 1.
[37] A. Birner, R.B. Wehrspohn, U.M. Gosele, K. Busch, Adv. Mater. 13 (2001) 177.
[38] N.D. Zakharov, P. Werner, U. Gosele, G. Gerth, G. Cirlin, V.A. Egorov, B.V. Volovik, Mater. Sci. Eng. B 87 (2001) 92.
[39] R.A. Soref, Proc. IEEE 81 (1993) 1687.
[40] J. Leuthold, C. Koos, W. Freude, Nat. Photonics 4 (2010) 535.
[41] K.Q. Peng, S.T. Lee, Adv. Mater. 23 (2011) 198.
[42] H.A. Atwater, A. Polman, Nat. Mater. 9 (2010) 205.
[43] J. Sun, H.T. Wang, J.L. He, Y.J. Tian, Phys. Rev. B 71 (2005) 125132(1).
[44] M.D. Segall, P.J. Lindan, M.J. Probert, C.J. Pickard, P.J. Hasnip, S.J. Clark, M.C. Payne, J. Phys. Condens. Matter 14 (2002) 2717.
[45] J.P. Perdew, K. Burke, M. Ernzerhof, Phys. Rev. Lett. 77 (1996) 3865.
[46] H.J. Monkhorst, J.D. Pack, Phys. Rev. B 13 (1976) 5188.
[47] M.L. Cohen, J.R. Chelikowsky, Springer Ser. Solid-State Sci. 75 (1989) 79.
[48] L.S.O. Johansson, P.E.S. Persson, U.O. Karlsson, R.I.G. Uhrberg, Phys. Rev. B 42 (1990) 8991.
[49] M. Cardona, F.H. Pollak, Phys. Rev. 142 (1966) 530.
[50] M. Vos, C. Bowles, A.S. Kheifets, M.R. Wen, Phys. Rev. B 73 (2006) 085207.
[51] R.O. Jones, O. Gunnarsson, Rev. Mod. Phys. 61 (1989) 689.
[52] A. Seidl, A. Görling, P. Vogl, J.A. Majewski, M. Levy, Phys. Rev. B 53 (1996) 3764.
[53] Z.H. Levine, D.C. Allan, Phys. Rev. Lett. 63 (1989) 1719.
[54] X. Gonze, C. Lee, Phys. Rev. B 55 (1997) 10355.
[55] D.M. Bylander, L. Kleinman, Phys. Rev. B 41 (1990) 7868.
[56] A.V. Krukau, O.A. Vydrov, A.F. Izmaylov, G.E. Scuseria, J. Chem. Phys. 125 (2006) 224106.
[57] F. Bechstedt, F. Fuchs, G. Kresse, Phys. Status Solidi B 246 (2009) 1877.
[58] J. Sánchez-Dehesa, J.A. Vergés, C. Tejedor, Phys. Rev. B 24 (1981) 1006.
[59] L.C. Kimmerling, H.J. Leamy, J.R. Patel, Appl. Phys. Lett. 30 (1977) 217.
[60] L. Ley, S. Kowalczyk, R. Pollak, D.A. Shirley, Phys. Rev. Lett. 29 (1972) 1088.
[61] S.K. Jain, P. Srivastava, J. Appl. Phys. 114 (2013) 073514.
[62] A.J. Read, R.J. Needs, Phys. Rev. B 44 (1991) 13071.
[63] J.T. Foley, U. Landman, Phys. Rev. B 14 (1976) 1597.
[64] H.R. Philipp, H. Ehrenreich, Phys. Rev. 129 (1963) 1550.
[65] G.K.M. Thutupalli, S.G. Tomlin, J. Phys. C, Solid State Phys. 10 (1977) 467.
[66] S.L. Adler, Phys. Rev. 126 (1962) 413.
[67] N. Wiser, Phys. Rev. 129 (1963) 62.
[68] M. Fox, Optical Properties of Solids, Oxford University Press, 1985, 66 pp.
[69] D. Lai, Y.H. Tan, C.S. Tan, Energy Proc. 8 (2011) 238.
[70] A. Antonelli, J.F. Justo, A. Fazzio, Phys. Rev. B 60 (1999) 4711.
[71] T.M. Schmidt, J.F. Justo, A. Fazzio, Appl. Phys. Lett. 78 (2001) 907.